Demonstration of real-time address header decoding for optical data routing at 1536 nm

T. L. Harris, Y. Sun, and R. L. Cone

Department of Physics, Montana State University, Bozeman, Montana 59717

R. M. Macfarlane

IBM Almaden Research Center, 650 Harry Road, San Jose, California 95120

R. W. Equall

Scientific Materials Corporation, 310 Icepond Road, Bozeman, Montana 59715

Received November 10, 1997

We have demonstrated real-time decoding of 20-bit biphase-coded address header pulses, using stimulated photon echoes in a phase-matched crossed-beam configuration. This decoding is one of the functions required for coherent transient optical data routing, packet switching, and processing. The active medium used was single-crystal Y_2SiO_5 doped with Er^{3+}, which provides an operating wavelength of 1536 nm. © 1998 Optical Society of America

OCIS codes: 060.4510, 070.4560, 160.2900, 160.5690, 030.1670.

One can exploit the frequency- and time-domain phenomena of spectral hole burning and photon echoes together with the ideas of spatial holography in spatial–spectral holography[1,2] to obtain optical storage and signal-processing capabilities that can be used separately or in powerful combinations. Real-time spatial–spectral holographic storage and processing of optical address headers was recently proposed[3] and experimentally demonstrated.[4,5] Those demonstrations were performed at the wavelengths of 580 and 793 nm with Eu- and Tm-doped insulating crystals, respectively. More recently, we showed[6] that erbium-doped insulating crystals, in particular Er^{3+}:Y_2SiO_5 (Er:YSO), have the required frequency-selective and coherence properties to provide operating wavelengths in the important 1550-nm telecommunications window. We report here our use of Er:YSO in a demonstration of address header decoding, one of several important components of high-speed data routing by optical packet switching[3–5,7,8] The advantages of optical packet switching[7] include fast data routing in the wavelength and space domains and transparency to packet bit rate and format. Specifically, we programmed a crystal to recognize biphase-coded address headers and to decode an arbitrary sequence of these headers, resulting in spatially discriminated optical output pulses. Each output pulse could be used to route or switch the optical data packet or the combined header and data packet in real time, requiring only a compact optical delay.

Address header decoding was performed in two stages.[3–5] First, the processing crystal was programmed with a distinct spatial–spectral holographic grating for each address header by the application of a pair of optical programming pulses, as shown in Fig. 1(a). This grating was stored by resonant Er^{3+} ions associated with the inhomogeneously broadened absorption of the Er:YSO spectral hole-burning material. The grating provides a simple way to visualize the stimulated photon-echo processing function. In the context of wavelength-division multiplexing, one can also store independent gratings at other adjacent wavelengths in the absorption profile. In this demonstration we programmed the crystal for two distinct biphase-coded address headers, labeled A and B, and two corresponding output directions, $\mathbf{k}_A$ and $\mathbf{k}_B$. The biphase-coded address-programming pulse for channel A propagated in the $\mathbf{k}_{\mathrm{add}}$ direction and was applied to the crystal just before the brief direction-programming pulse that propagated along $\mathbf{k}_A$. The direction-programming pulse was used to associate the $\mathbf{k}_A$ direction with address header A through the standard stimulated photon-echo phase-matching conditions of Fig. 1(c). The convolution of the address pulse and its brief direction pulse formed a spatial–spectral grating that the crystal stored for a time given by the stimulated photon-echo lifetime of the material, which is ~1 ms in this case but could be many orders of magnitude longer in materials that use a different hole-burning mechanism. The second grating, containing address B and its associated echo output direction $\mathbf{k}_B$, was programmed in the same manner as shown in Fig. 1(a).

The header processing stage is shown schematically in Fig. 1(b). Headers propagated along the $\mathbf{k}_H \equiv \mathbf{k}_{\mathrm{add}}$ direction, and each header generated stimulated photon-echo output signals following interaction with each stored grating. The phase-matching conditions $\mathbf{k}_{\mathrm{SE}}^{A(B)} = \mathbf{k}_H + \mathbf{k}_{A(B)} - \mathbf{k}_{\mathrm{add}}$, shown in Fig. 1(c), predict the emission directions $\mathbf{k}_A$ and $\mathbf{k}_B$ of the individual echoes. The shape of the stimulated echo is determined by the cross correlation of the header pulse with the convolution of the address- and direction-programming pulse pair stored in each

0146-9592/98/080636-03$15.00/0

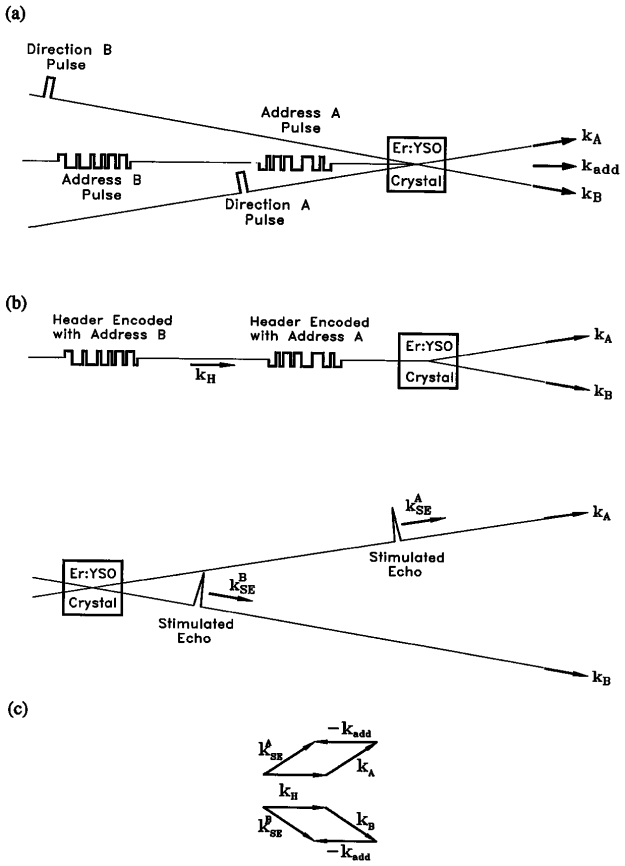

Fig. 1. (a) Temporal snapshot of the programming stage. For each header address, one spatial–spectral grating is stored in the crystal by a pair of programming pulses: a biphase-coded header address and a brief direction pulse. (b) Temporal snapshots of the processing stage. Headers coded with the addresses produce stimulated photon echoes in the spatial output channels that correspond to the directions programmed into the gratings by the brief direction pulses. (c) Phase-matching diagrams determining the wave vectors of the output stimulated photon echoes.

grating. Cross-correlation calculations predict that the echo produced along $\mathbf{k}_A$ by interaction of an A header with the A grating is dominated by a relatively strong narrow (~100-ns-duration, 1-bit-wide) central pulse and sidelobes that are more than an order of magnitude weaker. In addition, calculations predict that the unwanted cross-talk echo produced along $\mathbf{k}_B$ when header A interacts with grating B has no strong central peak but just weak sidelobes. With optimized codes, the cross correlation between headers can be minimized, thus minimizing the inevitable cross-talk echo. Processing of B code headers proceeded analogously.

The apparatus that we used is shown in Fig. 2. The external-cavity diode laser was home built and used the Littman configuration.[9] The output of the laser was coupled into an erbium-doped fiber amplifier. An interferometer wavemeter was used to monitor the laser wavelength with ±50 MHz accuracy. We focused the amplified beam into three 165-MHz acousto-optic modulators (AOM's) to produce three beams with nominal peak powers of 9 mW. A 1-GHz arbitrary waveform generator synthesized the 165-MHz carrier frequency for the electrical AOM drive pulses and controlled their phases and amplitudes.

The arbitrary waveform generator was programmed to produce two distinct 20-bit $\pm\pi/2$ biphase-coded address header pulses, A (−−+−−++−−−++−++−+−−) and B (−++−++−+−−+−−−+−−−++), of 2-μs total duration each (100 ns/bit). Direction-programming pulses of 100-ns duration, with no phase coding, followed the respective address-programming pulses by 3 μs. The programming pulse pairs were separated by 80 μs. The programming and processing stages were separated by 100 μs. Headers in the processing stage were incident at 9-μs intervals. The address header pulses were generated by AOM 2, and the direction-programming pulses by AOM's 1 and 3.

Output beams from the three AOM's were crossed at angles of ~70 mrad between adjacent pairs and focused to beam waists of radius $w_0 = 100$ μm in the crystal. The 0.001% Er:YSO crystal was mounted in a cryostat, and the decoding process was performed at a temperature of 1.5 K with a magnetic field of $H_0 = 8$ kG. Under these conditions, T_2 was ~150 μs, and the stimulated echo lifetime was ~1 ms. The Er:YSO crystal was oriented with its D_1 axis[10] parallel to H_0 and its b axis parallel to $\mathbf{k}_{\mathrm{add}}$. The laser was tuned to resonance with the Er^{3+} $^4I_{15/2}(1) \rightarrow {}^4I_{13/2}(1)$ transition at 1536.12 nm (site 1) in the Er:YSO crystal.[6] Stimulated photon echoes produced in the decoding process were detected by two 125-MHz-bandwidth InGaAs photodiodes, one for each output channel, and the outputs were fed into a digitizing oscilloscope for single-shot signal capture.

A representation of the temporal ordering (ABBABABA) of the 2-μs headers at 9-μs intervals is shown in Fig. 3(a). Single-shot data demonstrating header decoding are given in Fig. 3(b), which shows

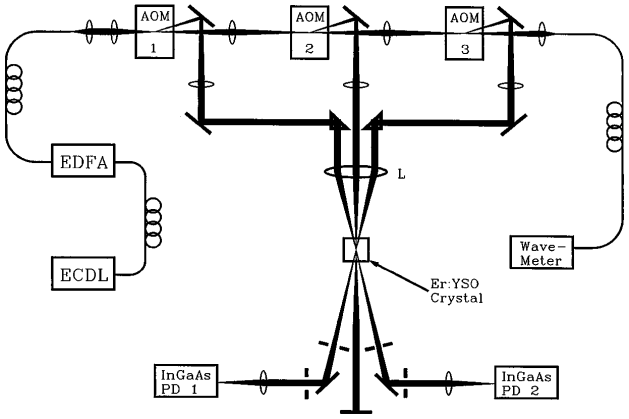

Fig. 2. Schematic of the experimental apparatus used for address header decoding. An external-cavity diode laser (ECDL) operating at 1536 nm is amplified by an erbium-doped fiber amplifier (EDFA) and gated by three AOM's to produce spatially separated beams that are crossed and focused in the crystal by lens L. Stimulated photon echoes are detected on the two InGaAs photodiodes (InGaAs PD 1, PD 2).

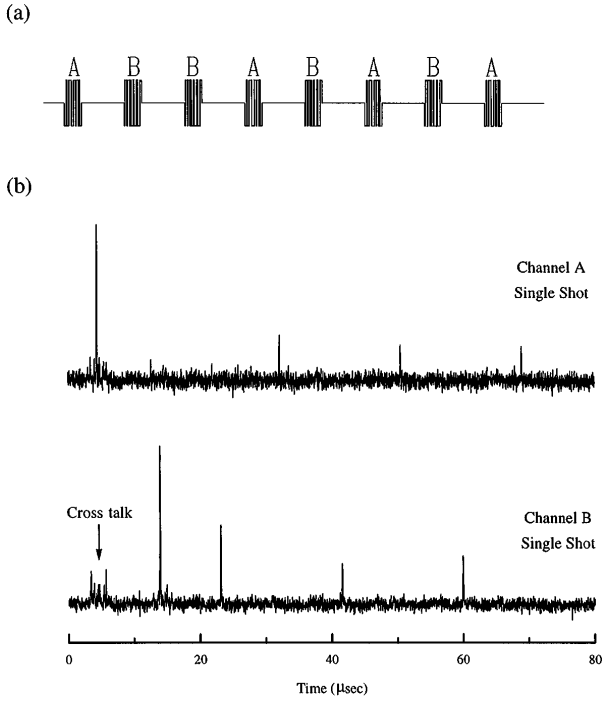

Fig. 3. (a) Representation of the header sequence in the processing stage, showing temporal ordering, spacing, and biphase coding of the header pulses. (b) Single-shot stimulated photon echoes detected during the header processing stage. Echoes are detected on channel A or B at a 3-μs delay after the application of the corresponding header; this delay is determined during the programming stage by the separation of the header programming pulse and the header direction programming pulse. Weak cross-talk echoes are also resolved from the noise.

the output of the A and B photodiodes. Stimulated photon echoes of 100-ns duration (the bit duration, as mentioned above) occur on each channel 3 μs after a correspondingly coded header passes through the crystal. Cross talk in the form of weaker stimulated photon-echo signals in the opposite channel was observed. This cross talk was due to the use of unoptimized header address codes, and it demonstrates the need to devise codes that minimize cross correlation between different headers.

We noted that the intensities of the decoded header pulses decayed in amplitude over the period of the processing. Increasing the time separation between the programming and processing stages resulted in the same accelerated decay of the pulse amplitudes during processing, but the overall signal levels showed the expected reduction owing to the material's intrinsic stimulated photon-echo decay. This result implies that the coded header pulses themselves are responsible for depleting the population difference that controls the echo intensity. Either reduction of the header pulse areas or the use of a gated processing material could reduce the decay of the output pulses that is due to this destructive readout.

In this signal-processing application there are several relevant time scales. During the programming step, coherence (determined by T_2) is required during only one header–direction pulse pair, and ideally the pulse pairs should be separated by more than T_2.[3–5] Typical values of T_2 for rare-earth-doped crystals are in the range 1–100 μs. In the processing step, the stimulated photon-echo decay places an upper limit on the length of the header pulse train that can be processed before reprogramming is required. Different applications will require different time scales; for example, in some cases one may want continuous routing with a fixed program, and in others one may wish to reprogram rapidly. In the implementation described here, the stimulated echo lifetime is ~1 ms, and T_2 is ~150 μs at the field of 8 kG. The stimulated photon-echo decay time depends on the mechanism for spectral hole burning and can be as long as hours or days in materials with a persistent hole-burning mechanism. In addition, photon-gated materials are known for other wavelength regions in which nondestructive readout is obtained.

In conclusion, we have demonstrated optical coherent transient–based real-time address header decoding for optical data packet routing and switching in the particularly important telecommunications window near 1550 nm. The observation of cross talk owing to unoptimized header codes demonstrates the need for codes that minimize cross correlations.

Research at Montana State University was supported in part by U.S. Air Force Office of Scientific Research grants F49620-94-1-0465 and F49620-96-1-0466 and by the National Science Foundation Experimental Program to Stimulate Competitive Research.

References

1. T. W. Mossberg, Opt. Lett. **7,** 77 (1982); W. R. Babbitt and T. W. Mossberg, Appl. Opt. **25,** 962 (1986).
2. A. Rebane, R. Kaarli, P. Saari, A. Anijdg, and K. Timpmann, Opt. Commun. **47,** 173 (1983); P. Saari, R. Kaarli, and A. Rebane, J. Opt. Soc. Am. B **3,** 527 (1986).
3. W. R. Babbitt and T. W. Mossberg, Opt. Lett. **20,** 910 (1995).
4. X. A. Shen and R. Kachru, Opt. Lett. **20,** 2508 (1995).
5. T. Wang, H. Lin, and T. W. Mossberg, Opt. Lett. **20,** 2541 (1995).
6. R. M. Macfarlane, T. L. Harris, Y. Sun, R. L. Cone, and R. W. Equall, Opt. Lett. **22,** 871 (1997).
7. For example, an overview was given by M. Renaud, F. Masetti, C. Guillemot, and B. Bostica, IEEE Commun. Mag. **35**(4)**,** 96 (1997).
8. K. D. Merkel and W. R. Babbitt, Opt. Lett. **21,** 71 (1996).
9. M. G. Littman and H. J. Metcalfe, Appl. Opt. **17,** 2224 (1978).
10. R. Beach, G. Albrecht, R. Solarz, W. Krupke, B. Comasky, S. Mitchell, C. Brandle, and G. Berkstresser, Proc. SPIE **1223,** 160 (1990); C. Li, C. Wyon, and R. Moncorge, IEEE J. Quantum Electron. **28,** 1209 (1992).